VIII International Conference on Particle-Based Methods
PARTICLES 2023
U. Perego, M. Cremonesi, A. Franci (Eds)

INVESTIGATION OF DYNAMIC CHARACTERISTICS OF ROLLING-BALL DAMPERS

KIRINO NAGASHIMA[1] AND MASATO SAEKI[2]

[1] Graduate School Engineering and Science, Shibaura Institute of Technology,
3-7-5 Toyosu, Koto-ku, Tokyo 135-8548, Japan

[2] Dept. of Mechanical Engineering, Faculty of Engineering,
Shibaura Institute of Technology
3-7-5 Toyosu, Koto-ku, Tokyo 135-8548, Japan
e-mail: saeki@sic.shibaura-it.ac.jp,
web page: https://www.particle.mech.shibaura-it.ac.jp/english

Abstract. Tuned mass dampers, consisting of a mass, spring, and damper, are widely used for vibration suppression in structures. Despite being small and lightweight, these dampers exhibit excellent damping effectiveness. However, there are issues such as performance degradation due to the aging of the spring and damper, as well as the need for frequent maintenance. Therefore, as an alternative vibration control device that does not rely on these components, a rolling-ball damper is proposed. This damper consists of a container with a lid and multiple enclosed particles on its curved surface. By utilizing the contact between particles and the friction between particles and the container, the rolling-ball damper can absorb and suppress the vibration energy imposed on the structure to which the container is attached. In this study, we investigated the characteristics of the rolling-ball damper in a horizontal vibration system. We experimentally verified the effects of the size and number of enclosed particles on damping performance. Furthermore, numerical simulations were conducted by the discrete element method using EDEM® software and the multibody dynamics simulation method using MotionSolve® software. A comparison between experimental and numerical simulation results demonstrated the effectiveness of numerical calculations in predicting the amplitude response.

Keywords: DEM, Dynamic Vibration Absorber, Granular Materials, Vibration Damper.

1 INTRODUCTION

Vibration in machinery and structures can lead to failures and collapse. Resonance phenomena, particularly when the natural frequency of a structure is close to the vibration frequency, can cause intense vibrations that result in significant damage to structures and machinery. Therefore, vibration control is of utmost importance. To address these issues, various damping devices are commonly employed. Among them, tuned mass dampers (TMDs) are the most widely used vibration control devices, consisting of a mass, spring, and damper. Despite being compact and lightweight, it exhibits a higher damping effectiveness than other damping devices. TMDs are widely utilized in a range of applications, from residential

structures to pedestrian bridges and chimneys. However, issues such as performance degradation due to the aging of the spring and damper, as well as the need for frequent maintenance, are associated with TMDs.

Komatsuzaki et al. have conducted research on the damping performance of a cycloid pendulum dynamic absorber. This damper has a simple structure with a cycloid-shaped surface and does not require frequent maintenance. However, in these dampers, adjusting the damping is challenging as it relies on varying the friction coefficient between the rolling body and the rolling surface. Tsuda et al. investigated the damping performance of a tuned rolling cylinder damper. This damper, which consists of multiple cylindrical rolling bodies loaded on a curved container, achieves good damping through the friction between the container and the rolling bodies. Chen et al. have experimentally demonstrated that a rolling-ball damper (RBD), in which multiple particles roll inside a spherical container, can effectively suppress the dynamic response of a wind turbine. Although they investigated in detail the damping effect, they focused on the motion of particles of the same size. Therefore, in this study, we investigated the characteristics of the RBD in a horizontal vibration system. This damper consists of a container with a curved surface and a lid, loaded with multiple particles. We experimentally verified the effects of the size and number of enclosed particles on damping performance. Additionally, numerical simulations were conducted using EDEM®-discrete element method (DEM) software and MotionSolve®-multibody dynamics simulation software. A comparison between the experimental and numerical simulation results confirmed the effectiveness of numerical calculations in predicting the amplitude response.

2 ROLLING-BALL DAMPER

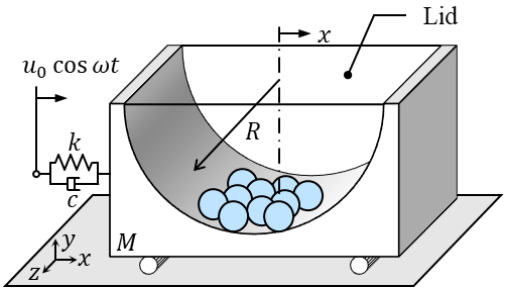

Figure 1: Model of experimental apparatus

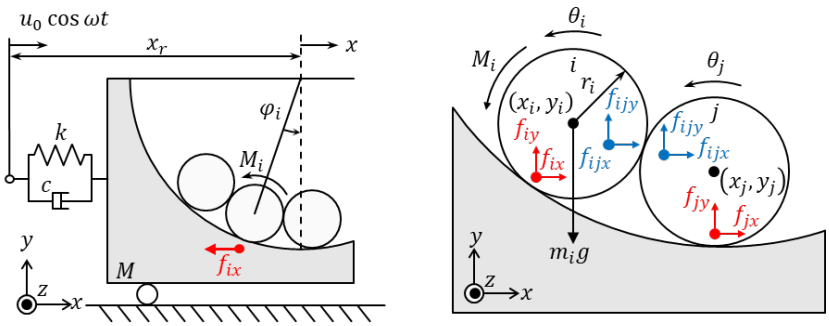

Figure 2: Analysis Model

Table 1: Parameters

Primary mass	M	Mass	x	Displacement
	c	Viscosity	f_{ix}	Contact force between the Primary mass and the Rolling element
	k	Spring constant		
	R	Radius		
Particles	m_i	Mass	I_i	Inertia moment
	x_i, y_i	Displacement	θ_i	Revolving angle of rolling element
	f_{ijx}, f_{ijy}	Contact force of Rolling elements	M_i	Contact torque
	r_i	Radius		
Excitation section	u_0	Vibration amplitude	ω	Frequency

Figure 1 shows a model of the RBD. The RBD consists of a curved surface incorporated into the primary mass, which contains enclosed particles. As the primary mass moves, the particles also move, and the contact force exerted by particles on the primary mass suppresses its vibration. Figure 2 shows the analysis model. The container consists of a curved surface with the radius of curvature R and a lid, where N particles are loaded on the arc. The primary mass with the mass M is connected to the excitation part through a tensile spring with the elastic constant k and a dashpot with the damping coefficient c. The primary mass is subjected to a sinusoidal displacement excitation $u_0 \cos \omega t$ in the excitation part. The equation of motion for the primary mass is as follows.

$$M\ddot{x}_r + c\dot{x}_r + kx_r + \sum_{i=1}^{N} f_{ix} = Mu_0\omega^2 \cos \omega t \tag{1}$$

The translational and rotational equations of motion for the i-th particle are as follows.

$$\begin{cases} m_i\ddot{x}_i = -f_{ix} + \sum_{j=2}^{N} f_{ijx} \\ m_i\ddot{y}_i = -f_{iy} + \sum_{j=2}^{N} f_{ijy} - m_i g \end{cases} \tag{2}$$

$$I_i\ddot{\theta}_i = M_i \tag{3}$$

Here, the particles are spherical with radii r_i, masses m_i, and moments of inertia I_i about their center of mass. The contact force exerted by the i-th particle on the primary mass is (f_{ix}, f_{iy}), and the contact force between the i-th and j-th particles is (f_{ijx}, f_{ijy}). The motion of the particles is analyzed by the DEM. The parameters are listed in Table 1.

3 EXPERIMENTAL APPARATUS

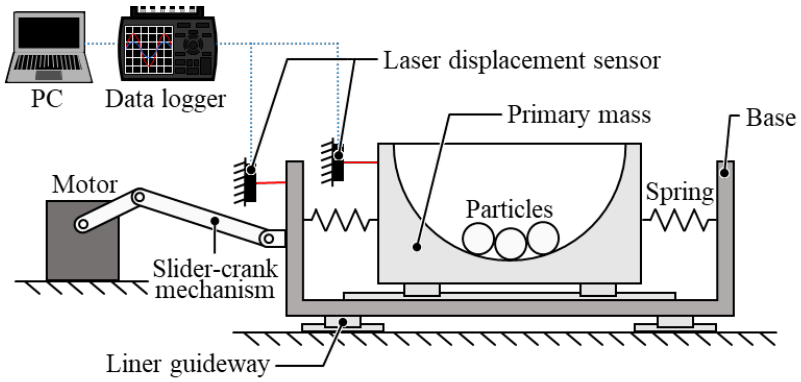

(a) Schematic of the experimental apparatus

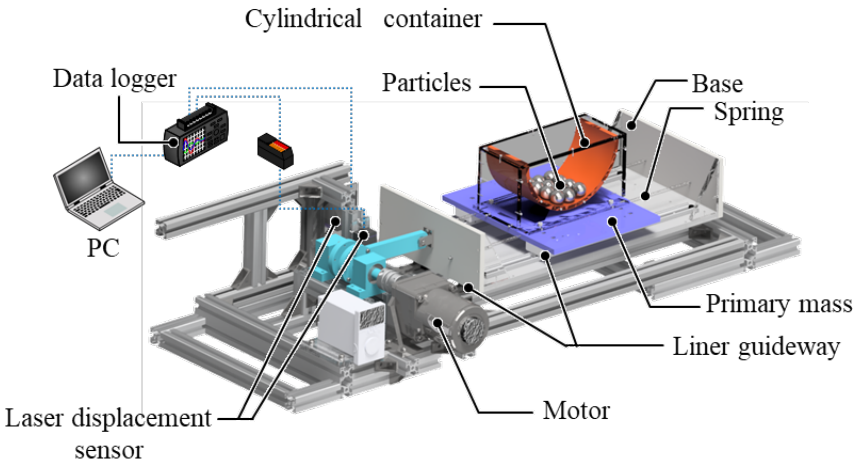

(b) CAD view of the experimental apparatus

Figure 3: Ezperimental apparatus

Table 2: Values of the system parameters

Frequency	0.57 - 2.08 Hz
Amplitude	8 mm
Arc radius	97 mm
Sampling time	1 msec

Figure 3 shows the experimental setup used in this study. The base oscillates the primary mass by receiving a sinusoidal excitation motion from a crank mechanism. The tensile spring is connected to the primary mass, providing a restoring force. A low-friction linear guideway is employed for the rectilinear motion of the primary mass, ensuring smooth translation. The linear guideway incorporates ball bearings attached to the slider, enabling smooth motion along the rail. Additionally, Table 2 shows the value of the system parameters.

4 EXPERIMENTS

4.1 Parameter estimation

The parameter estimation results for the vibration system without enclosing particles were obtained during the experiment. The equation of motion for the case without particle enclosure is presented below.

$$M\ddot{x}_r + c\dot{x}_r + kx_r = Mu_0\omega^2 \cos \omega t \tag{4}$$

We define the solution of the equation as $x_r = X_r \cos(\omega t - \varphi)$. When we consider the natural frequency ω_n, the damping ratio ζ, and the frequency ratio λ, the amplitude ratio X_r/u_0 can be determined as follows.

$$\frac{X_r}{u_0} = \frac{\lambda^2}{\sqrt{(1-\lambda^2)^2 + (2\zeta\lambda)^2}}$$
$$\tan \varphi = \frac{2\zeta\lambda}{1-\lambda^2} \tag{5}$$

$$\omega_n = \sqrt{\frac{k}{M}}\,, \zeta = \frac{c}{2\sqrt{Mk}}\,, \lambda = \frac{\omega}{\omega_n} \tag{6}$$

By using the Levenberg–Marquardt method, we performed an approximation for equation (4) based on the experimental results of the amplitude ratio without enclosing particles. The natural frequency ω_n and the damping ratio ζ were estimated. Furthermore, the value of each parameter was determined on the basis of the measured spring constant k, and the results are presented in Table 3. Figure 4 shows the amplitude response curve obtained from the estimated values in the table and the experimental results. As shown in the figure, the estimated values obtained by parameter estimation closely match the experimental values, indicating the validity of the results.

Table 3: Estimation Results

Primary mass M	2.94 kg
Natural frequency ω_n	1.46 Hz
Attenuation ratio ζ	0.0443
Attenuation coefficient c	2.39 N s/m
Spring constant k	248 N/m

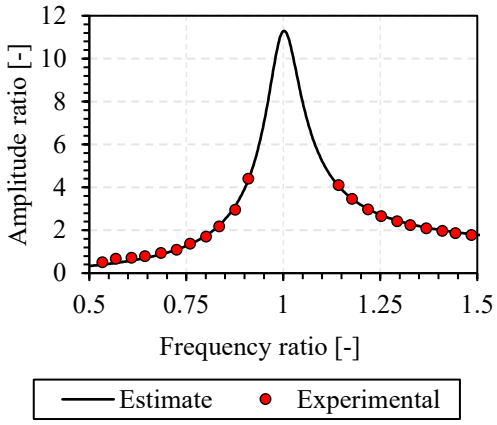

Figure 4: Amplitude response

4.2 Experimental results

In this section, we investigated the effects of the diameter of the enclosed particles and the ratio of the mass of the enclosed particles to the primary mass on the damping performance.

4.2.1 Effect of particle diameter

In this section, we examine the effect of the diameter of the enclosed particles on the damping performance. The mass ratio in all cases was set to 10%. Figure 5 presents the experimental results obtained. From the results, it can be observed that for a diameter of $\varphi 10$, the maximum amplitude ratio is 5.4, indicating the highest damping performance. Furthermore, the maximum amplitude ratio is around 7.5 for all particle sizes larger than $\varphi 15$.

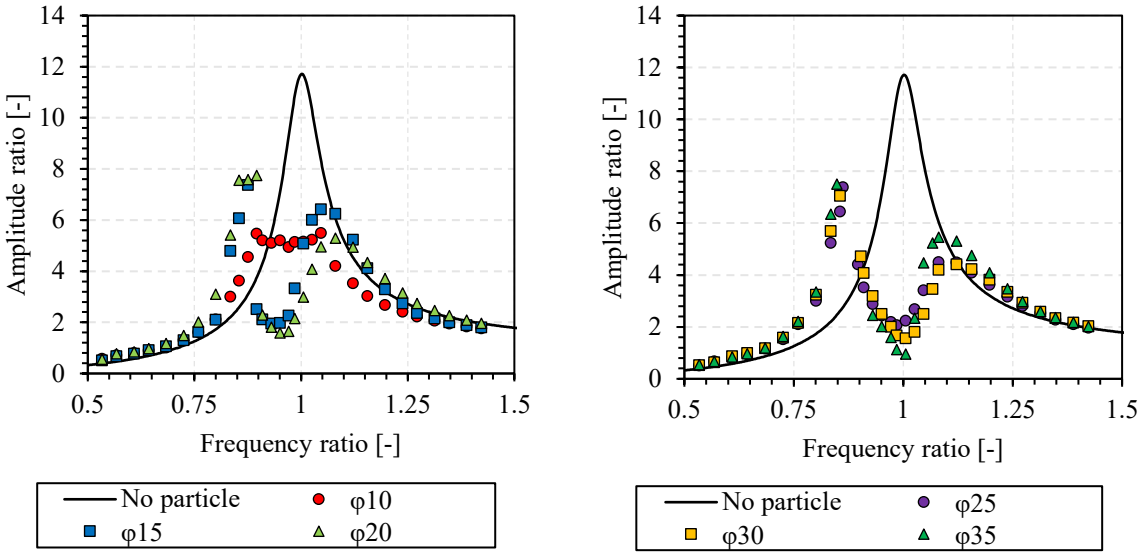

(a) $< \varphi 25$ mm (b) $\geq \varphi 25$ mm

Figure 5: Frequency response curve with various particle diameters (Mass ratio:10%)

4.2.2 Effect of mass ratio

In this section, we examine the effect of the mass ratio on damping performance. The particles used in the experiments have a diameter of $\varphi 10$. Figure 6 presents the experimental results obtained. From the results, it can be observed that for a mass ratio of 8%, the maximum amplitude ratio is 5.2, indicating the highest damping effectiveness. However, even at a mass ratio of 10%, a maximum amplitude ratio of 5.4 is obtained, indicating no significant difference. On the other hand, for a mass ratio of 13%, the maximum amplitude ratio is 7.3, indicating a significant decrease in damping performance. Therefore, it can be inferred that a mass ratio of 8–10% exhibits high damping effectiveness.

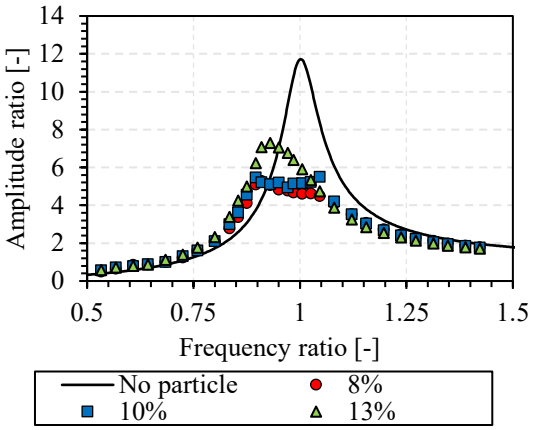

Figure 6:Frequency response curve with various mass rations ($\varphi = 10$ mm)

4.3 Enclosing particles of different materials and diameters

In this section, we present the experimental results obtained when enclosing particles of different materials and diameters. We experimentally investigated the combinations that result in higher damping performance under the current experimental conditions, and we present the combination that showed the most significant effect. The enclosed particles were glass balls with a diameter of φ25 and steel balls with a diameter of φ10. The mass ratio was set to 10%, and the ratio of the enclosed particles was 1 glass ball to 2 steel balls. Figure 7 illustrates the experimental results. From the results, it can be observed that a maximum amplitude ratio of 4.2 is achieved. This indicates that approximately 65% of the vibration is reduced compared with the maximum amplitude ratio without enclosing particles.

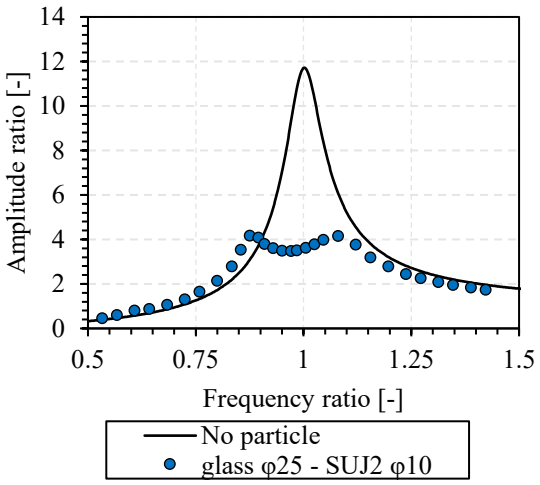

Figure 7: Frequency response curve with different size particles

5 NUMERICAL SIMULATION METHOD

5.1 DEM

In this study, contact force analysis between particles and between the container wall and particles was conducted by DEM. The method is a simulation technique for particles, in which the behavior of individual particles and their interactions, such as contact, collision, friction, and rotational motion, are considered.

5.1.1 Contact detection

It is necessary to define a contact detection equation for the determination of contact between particles and between the container wall and particles. In this section, we describe the contact criteria for both cases. In the formula, the proximity δ_n of two objects is used, and contact is considered to exist between two objects when $\delta_n > 0$.

(a) Particle to particle

The proximity δ_n is expressed as follows using the distance L_{ij} between the centers of the particles and the radius r_i of the particles.

$$\delta_n = (r_i + r_j) - L_{ij} \tag{7}$$

$$L_{ij} = \sqrt{(x_j - x_i)^2 + (y_j - y_i)^2 + (z_j - z_i)^2} \tag{8}$$

(b) Container wall to particle

The proximity δ_n is expressed as follows using the distance d from the center of the particle to the wall and the radius r of the particle.

$$\delta_n = r_i - d \tag{9}$$

5.1.2 Contact force calculation

The calculation of contact forces utilizes a method using the voigt model. This method is used to approximate the forces that occur during contact between particles and between the container wall and particles, using elastic and viscous forces. The contact forces are calculated individually for the normal directions and the tangential direction with respect to the contact surface. In this section, we will discuss the method for calculating contact forces separately in the normal and tangential directions.

(a) Normal direction

The calculation of contact forces in the normal direction is based on Hertz's contact theory and expressed as follows.

$$F_n = -k_n {\delta_n}^{\frac{3}{2}} - c_n \dot{\delta}_n {\delta_n}^{\frac{1}{2}} \tag{10}$$

In the above equation, the spring constant k_n varies depending on the contact between particles and the contact between the container wall and particles. It can be expressed by equations (11) and (12). Additionally, the damping coefficient can be represented by equation (13).

$$k_{n(p-p)} = \frac{\sqrt{2r}E_p}{3(1-{\nu_p}^2)} \tag{11}$$

$$k_{n(p-w)} = \frac{\frac{4\sqrt{r}}{3}}{\frac{1-{\nu_p}^2}{E_p} + \frac{1-{\nu_w}^2}{E_w}} \tag{12}$$

$$c_n = \alpha\sqrt{mk_n}{\delta_n}^{1/4} \tag{13}$$

$$\alpha = \frac{-\sqrt{5}\ln e}{\sqrt{(\ln e)^2 + \pi^2}} \tag{14}$$

(b) Tangential direction

The calculation of contact forces in the tangential direction is determined as follows.

$$F_t = -k_t {\delta_t}^{\frac{3}{2}} - c_t \dot{\delta}_t {\delta_t}^{\frac{1}{2}} \tag{15}$$

In the above equation, the spring constant k_t varies depending on the contact between particles and the contact between the curved container and particles. It can be expressed by equations (16) and (17). Additionally, the damping coefficient can be represented by equation (18).

$$k_{t(p-p)} = \frac{\sqrt{2r}E_p}{(2-\nu_p)(1+\nu_p)} \tag{16}$$

$$k_{t(p-w)} = \frac{4\sqrt{r}}{\frac{(2-\nu_p)(1+\nu_p)}{E_p} + \frac{(2-\nu_p)(1+\nu_p)}{E_w}} \tag{17}$$

$$c_n = \alpha\sqrt{mk_t}{\delta_t}^{1/4} \tag{18}$$

5.2 Software

In this study, numerical simulations were conducted using EDEM®-discrete element method software by Altair. Additionally, the method was combined with MotionSolve®-multibody dynamics simulation software.

6 NUMERICAL SIMULATION RESULTS

To assess the validity of the numerical simulation method described in the previous section, a comparison of its results with experimental results was conducted. Specifically, the comparison focused on the experimental results for the different enclosed particles discussed in Section 4.3. The parameters used in the analysis are presented in Table 4, and the analysis results are shown in Figure 8. From Figure 8, it can be observed that the maximum amplitude ratios obtained from the analysis closely match those obtained from the experiments. Although some discrepancies occur near the resonance points, the errors are minimal, suggesting that the analysis results are reasonable. From these findings, it can be concluded that EDEM enables the prediction of damping performance.

Table 4: Analysis Parameters

Particles	Material	Glass	SUJ2
	Mass	100 g	200 g
	Diameter	25 mm	10 mm
Frequency ratio range		1.22 ~ 1.81 Hz	
Analyze time		40 sec	
Calculation time step		1.5 μsec	
Sampling time		0.01	

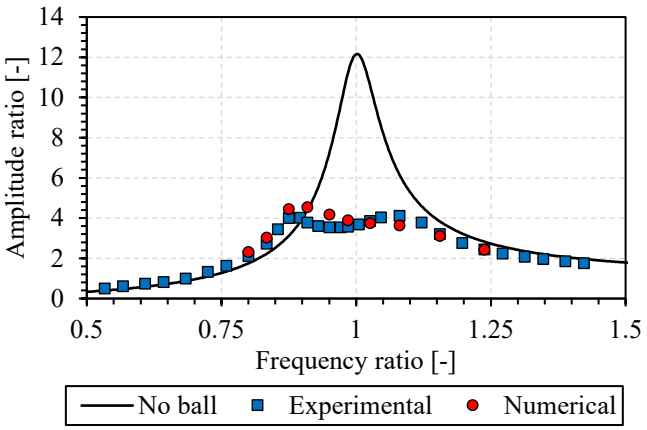

Figure 8: Experimental and numerical results

7 CONCLUSIONS

In this study, the damping performance of the rolling–ball damper was investigated by both experiments and numerical analysis. In the experiments, the effects of the diameter and mass ratio of the enclosed particles on the damping performance were examined. It was found that when using particles with a diameter of $\varphi 10$ and a mass ratio of 8%, approximately 55% of the vibration could be reduced. Furthermore, it was observed that the damping performance was improved by enclosing particles of different materials and diameters.

For the numerical investigation, EDEM® and MotionSolve® were used to predict the damping performance of the rolling–ball damper, the results of which were compared with those of experiments conducted under the same conditions to validate the numerical approach.

REFERENCES

[1] Komatsuzaki, T., Sato, H., Iwata, Y. and Ogawa, K. Study of cycloidal pendulum dynamic vibration absorber. *Transactions of the JSME (in Japanese)*, **72**, 716, 1049-1055 (2022).

[2] Tsuda, R. and Saeki, M. Efficiency of vibrational energy dissipation by tuned rolling‐cylinder dampers. *Journal of Sound and Vibration*, **463,** 114977 (2019).

[3] Ozawa, K. and Saeki, M. Study on damping performance of tuned rolling-cylinder dampers. *JSME Dynamics and design conference 2021 (in Japanese)*, **235** (2021).

[4] Chen, J. and Georgakis, C.T. Tuned rolling-ball dampers for vibration control in wind turbines. *Journal of Sound and Vibration*, **332**, 21, 5271-5282 (2013).